Phys Chem Minerals (2003) 30: 337–344
DOI 10.1007/s00269-003-0321-7



ORIGINAL PAPER

J. Maldener · A. Hösch · K. Langer · F. Rauch

# Hydrogen in some natural garnets studied by nuclear reaction analysis and vibrational spectroscopy

Received: 27 June 2002 / Accepted: 15 March 2003

**Abstract** A suite of 11 gem-quality, optically completely clear garnet crystals with a broad variety of compositions in the space of the end members pyrope–almandine–spessartine–grossular–andradite–goldmanite were analyzed for trace amounts of "water" by nuclear reaction analysis, NRA, based on the reaction $^{1}H(^{15}N, \alpha\gamma)^{12}C$, and by single-crystal absorption spectroscopy in the $\nu_{OH}$ vibrational range using microscope-FTIR-spectroscopic methods. The aim was to establish a calibration of the highly sensitive IR method with high areal resolution for "water" determination in garnets, by studying garnets of a wide compositional range, and to check for compositional dependencies of the integral molar absorptivities of the "water" component, $\varepsilon_{int}[1mol^{-1}_{H_2O}cm^{-2}]$, in the nominally "water"-free garnets. The results of NRA show a broad variation of water contents in the range (14 ± 3) to (950 ± 80) wt $ppm_{H_2O}$, the values being low and very high for the garnet solid solutions $(PyrAlm)_{SS}$ and close-to-end-member $Gross_{SS}$, respectively. There were no indications of inhomogeneities in the OH distribution, except possibly for one of the garnets (grossular, variety hessonite, from Tanzania). The quantitative evaluation of the complex $\nu_{OH}$ spectra, which showed similar shape only for members of the $(PyrAlm)_{SS}$, yielded integral absorption coefficients, $\alpha_{int}$ ($cm^{-2}$), which allowed the calculation of integral molar absorptivities, $\varepsilon_{int}$, using the "water" values of NRA. The $\varepsilon_{int}$ values obtained varied in a wide range but with no obvious correlation with the composition of the garnet except for the extremely high values, in the $10^4$ range, of the two specimen with compositions close to end-member grossular. In all other garnets, $\varepsilon_{int}$ was in the $10^3$ range with an average of $\varepsilon_{int} = 3630 \pm 1580[1mol^{-1}_{H_2O}cm^{-2}]$. Therefore, this value is proposed for the use in routine "water" determinations of compositionally different garnets by the micro-IR method, except for garnets near to end-member grossular.

**Keywords** Determination of hydrogen in garnets · Nuclear reaction analysis of hydrogen · Calibration of the IR-determination of hydrogen in garnets

J. Maldener · F. Rauch
Institut für Kernphysik, J. W. Goethe-Universität,
August Eular-Straße 6, 60486, Frankfurt am Main, Germany

J. Maldener (✉)
Kennedy Strasse 24a, 63477 Maintal, Germany
e-mail: joachim.maldener@t-online.de

A. Hösch · K. Langer (✉)
Institut für Angewandte Geowissenschaften,
Technische Universität Berlin, Ernst Reuter-Platz 1,
10587 Berlin, Germany

A. Hösch
Institut für Angewandte Geowissenschaften Technische
Universität Berlin, Ernst Reuter-Platz 1,
10587 Berlin, Germany

## Introduction

Solid–fluid interactions and product phases play a prominent role in the physicochemisty, geochemistry and mineral physics of Earth materials. In the elucidation of such interactions, the determination of trace hydrogen contents of nominally "water"-free[1] minerals is indispensble. As garnet is one of the most prominent phases of the Earth's upper mantle and transition zone, reliable date on trace "water" held in mantle garnets have been thoroughly studied for more than a decade (Ackermann et al. 1983; Aines and Rossman 1984a,b; Rossman et al. 1989; Geiger et al. 1991; Rossman and Aines 1991; Bell and Rossman 1992a,b; Beran et al. 1993; Langer et al. 1993; Rossman 1996; Lu and Keppler 1997; Matsyuk and Langer 1998; Geiger et al. 2000).

The most suitable experimental method for quantitative "water" determinations in minerals is to evaluate the intensity of the intrinsic OH valence vibrational

[1] Inverted commas indicate the structurally unspecified component water bound in the respective matrix.

**Table 1** Garnet crystals studied: sample designations, origin, properties, chemical composition quoted in terms of end-member fractions, as well as thickness, $t$ [cm] of plates prepared for FTIR microscope spectrometry

| Sample | Origin | Properties colour | Refractive index | Garnet end-member fractions, $x$[a] | | | | | | | $t$ (cm) |
|---|---|---|---|---|---|---|---|---|---|---|---|
| | | | | Pyr | Alm | Spess | Gross | Andr | Uw | Goldm | |
| RHOTAN1 | Tanzania | Deep red | 1.758 | 0.7494 | 0.2176 | 0.0036 | 0.0266 | 0.0000 | 0.0022 | 0.0006 | 0.4550 |
| PYALTAN | Tanzania | Deep red | 1.756 | 0.7104 | 0.2421 | 0.0075 | 0.0377 | 0.0000 | 0.0014 | 0.0009 | 0.1985 |
| RHOTAN2 | Tanzania | Deep red | 1.767 | 0.7022 | 0.2569 | 0.0068 | 0.0321 | 0.0000 | 0.0011 | 0.0009 | 0.2525 |
| HAI | Pakistan | Brownish red | 1.793 | 0.4507 | 0.5391 | 0.0040 | 0.0056 | 0.0000 | 0.0006 | 0.0000 | 0.4015 |
| RAJA | India | Brownish red | 1.793 | 0.4170 | 0.5359 | 0.0225 | 0.0237 | 0.0000 | 0.0009 | 0.0000 | 0.4021 |
| GTALX | Sri Lanka | Violet red | 1.770 | 0.4031 | 0.3531 | 0.1676 | 0.0278 | 0.0345 | 0.0139 | 0.0000 | 0.2015 |
| SPESSOR | Namibia | Orange | 1.798 | 0.0842 | 0.0275 | 0.8657 | 0.0198 | 0.0000 | 0.0028 | 0.0000 | 0.2009 |
| HESS1 | Tanzania | Red brown | 1.749 | 0.0000 | 0.0000 | 0.0000 | 0.8727 | 0.1098 | 0.0175 | 0.0000 | 0.0312<br>0.0165 |
| TSAV | Kenia | Emerald green | 1.749 | 0.0241 | 0.0000 | 0.0099 | 0.7764 | 0.0000 | 0.0267 | 0.1629 | 0.0515 |
| MALI | Mali | Grass green | 1.760 | 0.0310 | 0.0000 | 0.0033 | 0.7404 | 0.2162 | 0.0091 | 0.0000 | 0.2516 |
| GRMALI | Mali | Yellowish green | 1.762 | 0.0245 | 0.0000 | 0.0018 | 0.6499 | 0.3181 | 0.0057 | 0.0000 | 0.2000 |

[a] The end members are: *Pyr* pyrope $Mg_3Al_2[SiO_4]_3$; *Alm* almandine $Fe_3Al_2[SiO_4]_3$; *Spess* spessartine $Mn_3Al_2[SiO_4]_3$; *Gross* grossular $Ca_3Al_2[SiO_4]_3$; and *Andr* andradite $Ca_3Fe_2[SiO_4]_3$; *Uw* uwarowite $Ca_3Cr_2[SiO_4]_3$; *Goldm* goldmanit $Ca_3V_2[SiO_4]_3$

band or bands, $\nu_{OH}$ in the 2000–4000 $cm^{-1}$ range, because of the very high intensity of such bands resulting in detection limits down into the $ppm_{H_2O}$ range, and because of the availability of microscope-spectrometric IR methods which allow for areal resolution down to about 50 μm. The IR method uses the linear or integral absorption coefficient of the band or bands $\alpha_{lin} = \log(I_0/I)/t$ or $\alpha_{int} = (1/t)\int \log(I_0/I)d\nu$, respectively, where $\log(I_0/I)$ is the absorbance of the $\nu_{OH}$ band or bands and $t$ is the sample thickness in cm. Such data, which can be extracted from singe-crystal spectra, yield the "water" contents on the basis of the Lambert–Beer relation, which in the present case has the form:

$$C_{wt\%H_2O} = (\alpha_{lin,int}1.8)/(\varepsilon_{lin,int}D) \quad (1)$$

(e.g., Beran et al. 1993), where $D$ = density. It is obvious that the IR method and Eq. (1) apply only when hydrogen is not bound in very strong H bridges, which prevent $\nu_{OH}$ from showing up in the spectra (Beran and Libowitzky 1999). Such bridges do not occur in the present case of garnets. The linear or integral molar absorptivities of "water", $\varepsilon_{lin}(1mol^{-1}_{H_2O}cm^{-1})$ or $\varepsilon_{int}(1mol^{-1}_{H_2O}cm^{-2})$, respectively, depend on chemical and structural peculiarities at the sites where hydrogen is bound to oxygen in the respective mineral structure. Therefore, calibrations of the molar absorptivities of $\nu_{OH}$ are needed. These were performed on the mineral of interest by independent and highly sensitive methods of "water" determination.

In the case of garnets, Rossman and Aines (1991) obtained a calibration for OH-bearing-grossular, $\varepsilon_{int} = 7500(1mol^{-1}_{H_2O}cm^{-2})$, and Bell et al. (1995) for an $OH^-$-bearing calcic pyrope–almandine garnet–megacryst from Monastery/South Africa (MON9), $\varepsilon_{int} = 6700 \pm 670(1mol^{-1}_{H_2O}cm^{-2})$. The independent values of the "water" contents in both garnets were obtained by extraction and manometry of hydrogen. The latter $\varepsilon_{int}$ value was used for "water" determinations by the IR method, on a large number of garnets from mantle xenoliths from southern Africa (Bell and Rossman 1992a,b) and Yakutia/Siberia (Matsyuk and Langer 1998). The results obtained in these studies rely on the applicability of the $\varepsilon_{int}$ value used for the garnets under study. Their composition may differ from that of the calibrational garnet. Differences in their crystal chemistry may alter the specific molar "water" absorptivity, as already shown previously (Aines and Rossman 1984; Rossman et al. 1998; Rossman and Aines 1991).

In order to elucidate such effects and to obtain $\varepsilon_{int}$ values for garnets of different chemical composition, a series of 12 natural garnet crystals was studied by nuclear reaction analysis, NRA, using the reaction $^1H(^{15}N,\alpha\gamma)^{12}C$ for the independent calibrational determinations of the "water" contents (Wagner et al. 1989; Endisch et al. 1993, 1994; Maldener et al. 2001) of the crystals and by single-crystal vibrational spectroscopy in the energy range of the $\nu_{OH}$ fundamentals.

## Experimental

### Samples

The samples studied, listed in Table 1[2], were crystal plates ground from irregularly shaped fragments of garnet crystals, with dimensions of up to 0.5 cm. These garnets all had gemstone quality, were all optically isotropic and showed no effects of internal strain, zonation of colour or inclusions of other minerals and fluid phases when studied under the polarizing microscope. In every case, all plates contained areas well in excess of 60 × 60 μm – the size of the measuring spot selected – free from inclusions and fractures. After grinding to a thickness appropriate to obtain absorbancies below 3,000 in the spectral range 4000–2000 $cm^{-1}$, the plates were polished from both sides. All plates were examined by several core-rim lateral IR scans and also by vertical scans using IR and NRA methods (see below). No inhomogenities of H distribution were detected.

[2] The origin of the samples studied cannot be described more precisely than in Table 1, because the mines or mine districts are not known to the authors. On the other hand, all experience shows that crystals from the same mine are often different in their $\nu_{OH}$ bands and "water" contents. For further reproductions of our results, we shall try to make provisions to lend out a sample on request.

The chemical compositions of these plates were obtained by means of X-ray fluorescence analyses (BRUKER SRS3400, Rh tube operated at 60 KeV, LiF/PF/Pb-stearate crystals as monochromatizers, external silicate standards of the Bundesanstalt für Materialforschung, Berlin). The compositions obtained are recalculated as mole fractions of garnet end members and listed in Table 1. It is obvious from such data that the samples can be grouped as pyrope–almandine solid solutions (RHOTANI, PYRALTAN, RHOTAN2, HAI, RAJA), spessartine (SPESSOR) and andraditic or goldmanitic grossular solid solutions (HESS1, MALI, GRMALI, TSAV). Elements other than those of the end members quoted in Table 1 were present, if at all, in the $\leq 0.02\%$ range. Approximate densities D (g $cm^{-1}$) needed in the evaluation of Eq. (1), were obtained on the basis of the Winchell diagrams from composition and refractive indices of the garnet plates.

## H determination by nuclear reaction using the $^1H(^{15}N,\alpha\gamma)$ reaction

The principles of the method have been described before (Wagner et al. 1989; Endisch et al. 1993, 1994; Maldener et al. 2001). In brief, the plane-polished sample under study is bombarded with a beam of high-energy $^{15}N$ ions. The presence of hydrogen in the sample is indicated by the emission of $\gamma$-rays with the characteristic energy of 4.4 MeV. The yield of these $\gamma$-rays is recorded dependent on the energy of the accelerated $^{15}N$ ion beam. The yield curve obtained can be converted into a concentration-depth profile after calibration of the setup with a suitable standard. The depth range of the method is 2 μm. In a typical concentration-depth profile, the hydrogen concentrations decrease at increasing depths from the surface to lower parts so that a plateau of depth-independent concentrations is formed. The high values at the surface and shallow depths are caused by the distributed surface layer of the sample, the Beilby layer (Beilby 1921; Bowden and Hughes 1937a,b). The interpolated concentration value of the plateau can be regarded as typical of the concentration in the bulk sample, provided hydrogen is otherwise homogeneously distributed. From the nuclear reaction scheme (see above), it is clear that the experiments provide hydrogen concentrations $c_H$, which in the case of oxygen based material are recalculated to "water" concentrations $c_{H_2O}$.

The NRA measurements of the present paper were performed using the 7 MeV van de Graaff accelerator of the Institut für Kernphysik, Frankfurt am Main. The measuring setup used is a modified version of that described by Endisch et al. (1993, 1994). The modifications include a sputter gun for in-situ sample cleaning and a movable sample holder which enables positioning of a sample relative to the 15N ion beam. A detailed description will be given elsewhere (J. Maldener, F. Rauch, personal communication). Profiling measurements were taken at several energies of the $^{15}N$ ion beam in the range of 6.4 to 10.0 MeV corresponding to a depth range of 0 to 1500 nm. The beam spot on the sample was defined by a collimator so that diameters between 1 and 2 mm could be chosen, depending on the size of the sample.

All samples except for RHOTHAN2 and HAI (Table 1), were analyzed on two different spots, either on the same side of the plates or on the front and back side. Samples GTLAX, SPESSOR and GMALI (Table 1) were analyzed for a third time on one of the two facing sides, on a new spot after removing a surface layer of about 500 nm by prolonged sputtering. Sample HESS was also analyzed for a third time, in this case after polishing away a layer 160 μm thick.

A polymer foil with known stoichiometric hydrogen content (Kapton) served as standard in the calibration of the NRA procedures. The relative systematic error of the "water" contents obtained by the NRA methods sketched here is ± 8% (Maldener et al. 2001). In measurements on blanks (Si or $Al_2O_3$ wafers), a small beam-induced background count rate corresponding to 2 ± 2 wt.ppm $H_2O$ was observed which varied with time and beam energy. This background could be ascribed to reactions of the $^{15}N$ ion beam with the beam collimator or other parts of the beam line. More details of the procedures are presented elsewhere (Maldener et al. 2001)

## $\nu_{OH}$ Vibrational spectroscopy and evaluation of spectra

Vibrational spectra of the garnets were obtained on the polished plates listed in Table 1, using a Fourier transform interferometric spectrometer (BRUKER IFS66) which provides a high spectral resolution of down to 0.25 $cm^{-1}$ and is equipped with a Globar light source, a KBr beamsplitter and a mirror drive of high accuracy. The instrument is permanently flushed with dry, $CO_2$-free air at 120 kPa. An IR microscope (BRUKER IR Scope 1) is attached to the spectrometer. The microscope is equipped with 15 × Cassegrain-type mirror optics enabling measurements on sample spots down to 30 × 30 μm. A $LN_2$-cooled MCT-type B serves as detector in the optical ocular position of the microscope. This IR microscope was permanently flushed with pure Ar at 200 kPa. All single-crystal spectra were measured under ambient conditions.

The entire spectral range accessible with the above beam splitter, 7000–400 $cm^{-1}$, was scanned repeatedly – the $\nu_{OH}$-specific range 3800–3300 $cm^{-1}$ in abscissa-expanded mode – operating the instrument at a spectral resolution of 2 $cm^{-1}$; 130 scans were averaged. As the band widths, i.e., the full widths at half maximum of the computer-resolved component bands of the complex $\nu_{OH}$ spectral envelopes, were in the range of 6 to 60 $cm^{-1}$, errors due to finite spectral slit widths are insignificant (Ramsey 1952). Measuring spots were 60 × 60 μm to achieve high measuring intensity. The calculational curve resolutions (program OPUS version 2.0 by BRUKER) of the complex $\nu_{OH}$ band envelopes obtained for the garnets of Table 1, were based on the constraints used by Matsyuk and Langer (1998), who used the same instrument and methods of crystal-slab preparation in their garnet work. The spectral background was subtracted by using an "elastic band", i.e., a Bezier function, which could be selected to fit the observed background and was chosen such that a broader wavenumber range was fitted than that in which all the garnet $\nu_{OH}$-bands occurred.

To evaluate the "water" contents of the samples from the integral absorption coefficients $\alpha_{int}$ to be extracted from the single-crystal $\nu_{OH}$ spectra, Eq. (1) is to be used, which involves the plate thicknesses $t$ to calculate $\alpha_{int}$ from the integral absorbancies $\int \log(I_0/I)\mathrm{d}\nu$, obtained from the spectral envelopes by the curve resolution procedures. To use measured plate thickness $t_{pl}$ is correct only under the condition that parallel measuring radiation is impinging a plate with plane-parallel surfaces under an angle of 90°. Only in this case is the crystal volume penetrated by the measuring beam a cylinder, the volume of which is directly related to the thickness $t_{pl}$. However, the measuring radiation of the microscope-spectrometer is convergent and thus forms a truncated cone inside the plate. The volume of this cone is larger than that of a $t_{pl}$-proportional cylinder, the thicker the plate the more. To account for this, a correction of $t_{pl}$ was approximated as follows.

In the microscope[3], the convergent measuring beam impinges the plate to be measured from below. When the focus is set to the upper surface of the plate, the upper area of the truncated cone is identical with the area of the measuring spot with diameter $d_{meas}$. Then for the case that the medium in which the measuring beam travels before impinging the sample, is air with $n_{air} \cong 1{,}000$,then the diameter of the lower area of the truncated cone $d_{div}$ can be calculated from the angle of incidence $i$, the refractive index of the sample $n_s$ and the angle of refraction $r$, where $r$ and $i$ are connected with each other by Snell's law:

$$r = \arcsin(\sin \mathrm{i}/n_s) \quad (\text{for } n_{air} = 1{,}000, \text{free-carrying sample plate}) \tag{2}$$

[3] The following line of argumentation holds for transmission objectives. However, it applies also for mirror objectives despite their dark central area when relative intensities are measured, as is the case in absorption spectroscopy, recording transmission, $I/I_0 = T$, or absorbance, $\log(I_0/I)$.

$$d_{\mathrm{div}} = d_{\mathrm{meas}} + (2 * t_{\mathrm{pl}} * \tan r) \quad (t_{\mathrm{pl}} = \text{thickness of the sample plate}), \tag{3}$$

and the volume of the truncated cone-shaped beam inside the sample, $V_{\mathrm{tcs}}$,is

$$V_{\mathrm{tcs}} = (1/12)\pi t_{\mathrm{pl}}(d_{\mathrm{div}}^2 + d_{\mathrm{div}}\, d_{\mathrm{meas}} + d_{\mathrm{meas}}^2). \tag{4}$$

The values of $d_{\mathrm{div}}$ and $d_{\mathrm{meas}}$ are averaged to obtain a mean diameter of the beam $d_{\mathrm{av}}$ This value and the $V_{\mathrm{tcs}}$ as calculated by Eq. (4) are used to calculate the length of a cylinder of a volume equal to $V_{\mathrm{tcs}}$. This length is the divergence-corrected, effective plate thickness $t_{\mathrm{corr}}$, which is to be used in Eq. (1) instead of the direct plate thickness $t_{\mathrm{pl}}$.

$$t_{corr} = 4 * V_{tcs}/(\pi * d_{av}) \tag{5}$$

As an example, the deviation between integral absorption coefficients obtained with uncorrected $t_{\mathrm{pl}}$ and divergence-corrected $t_{\mathrm{corr}}$ is shown in Fig. 1 as a function of the diameter of the measuring area, for a plate of garnet HESS1 with $t_{\mathrm{pl}} = 0.0567$ cm. The ordinate values are the sums of the integral absorption coefficients of all component OH–valence vibrational bands as determined by curve decomposition of the OH spectrum.

## Experimental results and discussion

Hydrogen depth profiles of four of the garnets of Table 1, which are typical of the whole garnet series studied here, are shown in Fig. 2, where the hydrogen concentration is expressed as wt.ppm $H_2O$. Error bars indicate the typical statistical error of single data points.

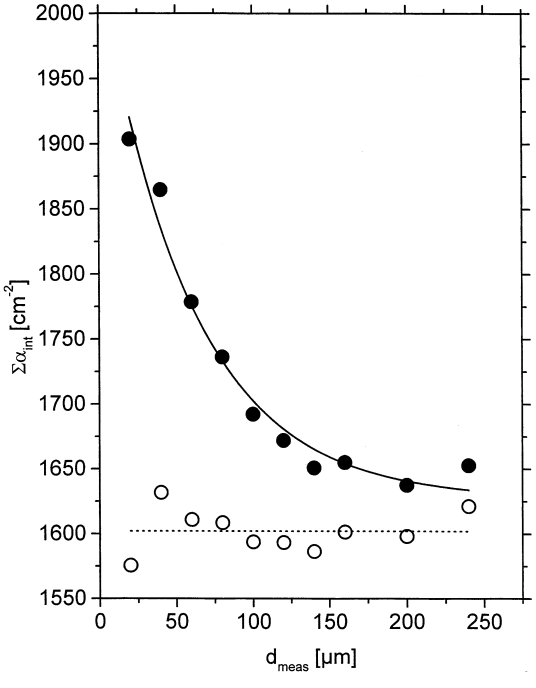


**Fig. 1** Deviation between the sum of integral absorption coefficients $\alpha_{\mathrm{int}}$ of the $\nu_{\mathrm{OH}}$ band system in HESS1 (Table 1) with 12 analyzed component $\nu_{\mathrm{OH}}$ bands, as determined either using the measured plate thickness t = 0.0567 cm, *closed symbols*, or the divergence-corrected thickness $t_{\mathrm{corr}}$ as obtained by the formalism of Eqs. (2) to (5), *open symbols*. Values of $\Sigma\alpha_{\mathrm{int}}$ are plotted as functions of the diameter of the measuring area focused at the upper surface of the crystal plate (see text)

Some profiles show high data points at low depths due to hydrogen-bearing defects produced in the surface of the plates on grinding and polishing. Figure 2 shows such effects for the garnets GRMALI and, though less clearly, RAJA. The data evaluation was limited to a correspondingly smaller depth range. The limits chosen in the case of the garnets of Fig. 2 are shown by the dashed vertical lines. To evaluate the concentration of "water" for a specific sample, all data points at depths greater than the position of the vertical line were averaged without distinguishing the two or three data sets from the different profiling measurements. This procedure is justified, since in all cases the averages of the different data sets on the same sample agree within their statistical uncertainties. For the sample HESS1, the profiling data points obtained after removal of a 160-μm-thick layer were averaged separately because of the different values of the integral $\nu_{\mathrm{OH}}$-absorbance obtained for the original and the thinned plate (see below). The "water" concentration values found by such evaluations of the profiles were corrected for the background measured on blanks, i.e., by subtracting 2 wt.ppm$_{H_2O}$. The "water" values obtained are summarized in Table 2. The errors quoted include the statistical error connected with the averaging procedure of the data points in the respective profile, as well as the systematic error arising from the calibrational procedure.

The infrared absorption spectra after subtraction of background as described above, in the $\nu_{\mathrm{OH}}$ vibrational range of the garnet crystal plates are displayed in Fig. 3 and 4. Figure 3 presents the spectra of those garnets of Table 1 which were grouped as pyrope–almandine solid solutions in the section on the samples. Figure 4 displays spectra of those samples of Table 1 which are summarized as spessartine, grossular–andradite (SPESSOR, HESS1, MALI, GRMALI) or grossular–goldmanite solid solutions (TSAV).

The shapes of the spectra of the upper part of Fig. 3 are nearly identical, though band intensities differ. The three spectra exhibit, apart from some very small features, a band system centred near 3540 cm$^{-1}$ with a maximum near 3550 cm$^{-1}$ and a strong shoulder at ca.3530 cm$^{-1}$. The spectra of HAI and RAJA in the lower part of Fig. 3 are very similar to each other, again except for the intensities. They also resemble those of the first three samples in that they exhibit a band system close to 3530 cm$^{-1}$, again with a strong maximum centred close to 3540 cm$^{-1}$ and a band doublet at 3525 cm$^{-1}$, which might correspond to the shoulder in the former three spectra. This doublet is more intense in the spectra of the latter samples than the shoulder in the former ones. The spectrum of GTALX in the lower part of Fig. 3 differs strongly from those of HAI and RAJA in that this spectrum shows two band systems, I, centred at ca 3650 cm$^{-1}$ and II, centred at 3560 cm$^{-1}$. The maximum of system I, occurs at 3652 cm$^{-1}$ with an inflection at 3637 cm$^{-1}$, while the maximum of system II, is at 3560 cm$^{-1}$ with a strong and broad shoulder at 3600 cm$^{-1}$. Perhaps this spectrum of GTALX differing

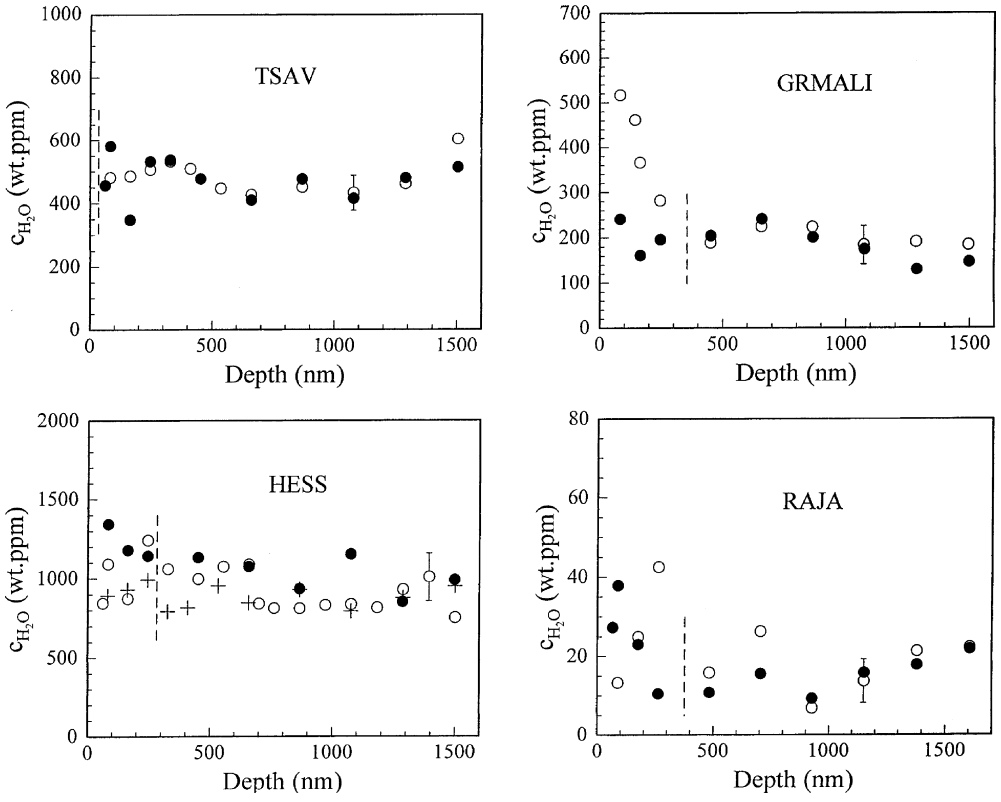


**Fig. 2** Hydrogen depth profiles obtained in $^{15}N$ NRA measurements on four of the garnet samples studied, representative for the whole suite of 11 garnets. The *open and full circles* denote data from the first and second profiling measurement, respectively. The *crosses* denote data obtained for HESS1 after removal of 160 μm from the total thickness of the plate. *Error bars* represent typical statistical errors of individual data points. *Vertical dashed lines* indicate the lower end of the depth ranges used for obtaining the averaged $c_{H_2O}$ values. These lines can be regarded as limit between the surface layer disturbed by cutting, grinding and polishing the crystal fragments, i.e., their Beilby layer, and the undistributed crystalline matrix

**Table 2** "Water"[a] concentrations $c_{H_2O}$ as obtained by NRA, integral absorption coefficients $\alpha_{int}$ of the $\nu_{OH}$ vibrational band system in the single-crystal spectra of the garnets studied (Table 1), and integral molar absorptivities $\varepsilon_{int}$ of "water" in the garnets, as calculated from $c_{H_2O}$ and $\alpha_{int}$. The values of $\alpha_{int}$ were calculated from integral absorbancies using divergence-corrected plate thickness $t_{corr}$ (cf. $t_{corr}$ with uncorrected, measured $t$ values quoted in Table 1); $D$ density; $M$ molar weight of the respective garnet

| Sample | $M$ | $D$ (g cm$^{-1}$) | $c_{H_2O}$ (wt.ppm$_{H_2O}$) | $t_{corr}$ (cm) | $\alpha_{int}$ (cm$^{-2}$) | $\varepsilon_{int}$ (l mol$_{H_2O}^{-1}$cm$^{-2}$) |
|---|---|---|---|---|---|---|
| RHOTAN 1 | 425.6 | 3.743 | 19 ± 4 | 0.5804 | 20 | 5000 |
| PYRALTAN | 428.8 | 3.764 | 17 ± 4 | 0.2424 | 7 | 1960 |
| RHOTAN 2 | 429.8 | 3.775 | 18 ± 4 | 0.3129 | 13 | 3440 |
| HAI | 454.9 | 3.981 | 18 ± 4 | 0.5092 | 25 | 6340 |
| RAJA | 457.1 | 3.990 | 14 ± 3 | 0.5100 | 10 | 3230 |
| GTALX | 455.0 | 3.985 | 48 ± 10 | 0.2460 | 25 | 2370 |
| SPESSOR | 486.5 | 4.128 | 25 ± 5 | 0.2451 | 28 | 4880 |
| HESS (thick) | 457.7 | 3.616 | 950 ± 80 | 0.0329 | 2006 | 10600 |
| (thin) | | | 870 ± 90 | 0.0169 | 2510 | 14400 |
| TSAV | 458.9 | 3.615 | 480 ± 40 | 0.0564 | 1208 | 12600 |
| MALI | 462.1 | 3.648 | 170 ± 20 | 0.3118 | 168 | 4800 |
| GRMALI | 468.1 | 3.676 | 190 ± 20 | 0.2443 | 77 | 2030 |

[a] The inverted commas indicate the structurally unspecified component water in the respective garnet matrix

so strongly from the others shown in Fig. 3 is related to the fact that GTALX contains a high amount of the spessartine end member, while all others are very low in the spessartine component, which is also true for the grossular component (Table 1). On the other hand, there is no similarity between the spectrum of the spessartine-bearing pyrope–almandine solid solution GTALX (Fig. 3, lower part) with that of spessartine SPESSOR shown in the upper part of Fig. 4. The upper and lower parts of Fig. 4 display the spectra measured on SPESSOR and on the four grossular-rich garnet solid solutions of Table 1, HESS1, MALI, GRMALI and TSAV. The andradite contents of the grossular-rich solid solutions HESS1, MALI and GRMALI increase in the sequences of these samples, otherwise they are chemically quite similar (Table 1). From this, one might expect their $\nu_{OH}$ spectra to be similar and to exhibit gradual changes. However, this is the case for the two latter garnets only while the spectra of HESS1 resemble that of the andradite-free but goldmanite-bearing TSAV (Fig.4, lower part). There is no straightforeward explanation for all these spectral variations.

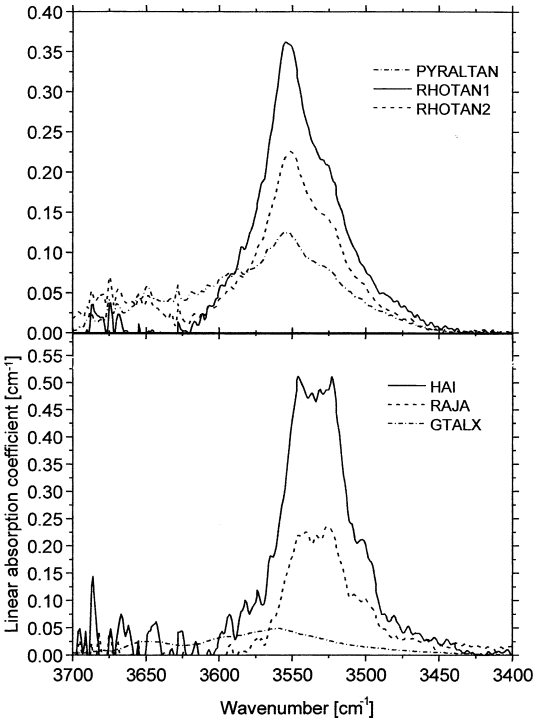


**Fig. 3** Single-crystal spectra in the $\nu_{OH}$ vibrational range at ambient conditions, of the group of pyrope–almandine garnet-rich solid solutions of Table 1. The *upper part* shows spectra obtained on garnets with pyrope fractions above 0.7, the *lower part* those of garnets with pyrope fractions below 0.5. Plotted are the linear absorption coefficients, $\alpha_{lin}$, normalized to $cm^{-1}$ using the divergence corrected thickness $t_{corr}$, over the wavenumber of the measuring radiation in $cm^{-1}$. The spectra are background-corrected by the Bezier function (cf.text)

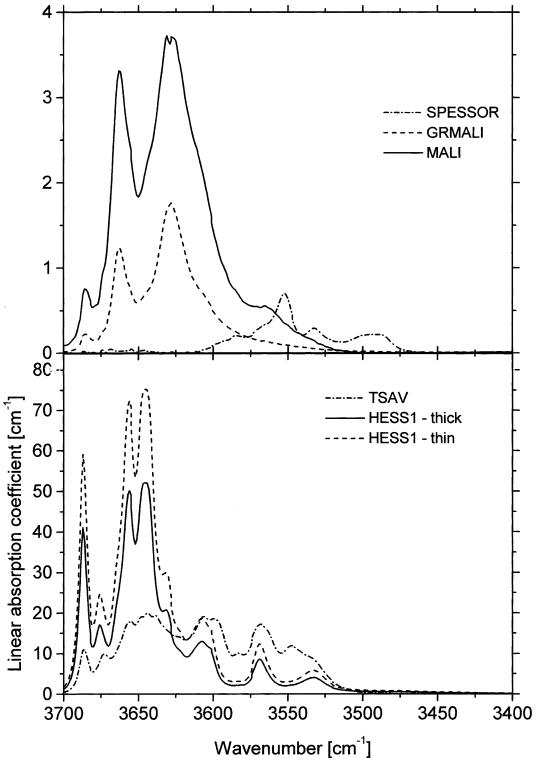


**Fig. 4** Single-crystal spectra in the $\nu_{OH}$ vibrational range at ambient conditions, of spessartine and andraditic grossulars, *upper part*, and of grossulars, *lower part*. The sample designations are those of Table 1. The spectra are plotted as in Fig. 3

Though a structural interpretation of the observed bands is highly desirable, such an interpretation is not a necessary condition for the task of the present paper, namely to calibrate the integral $\nu_{OH}$ intensity against the "water"' contents. This is valid as long as it can safely be assumed that all $\nu_{OH}$ are intrinsic and not in part caused by $OH^-$ in inclusions, on fractures or dislocations. That this is not the case for our samples was ensured by microscopic examination of the optically completely clear parts where the IR measurement spots were set on the gem-quality crystal plates (see above).

Thus, the integrated $\nu_{OH}$ intensities in the wavenumber range 3700 to 3400 $cm^{-1}$ were used to calculate the integral molar absorptivities, $\varepsilon_{int}(1mol^{-1}_{H_2O}cm^{-2})$ according to Eq. (1). The error in the $\alpha_{int}$ values due to the uncertainties in the background corrections is estimated to be $\pm$ 3 to $\pm$ 8% on the basis of repeated measurements and processings of the same spectra. All the data used to obtain the $\varepsilon_{int}$ values and these values themselves are listed in Table 2. We should note that we quote the simple $\varepsilon_{int}$ values in Table 2, whereas some authors prefer to use 3 $\varepsilon_{int}$ (Paterson 1982; Libowitzky and Rossman 1997). These authors wish to be consistent with summing up all three $\varepsilon_{int}$ values obtained for the three major optical directions $X(\alpha)$, $Y(\beta)$, $Z(\gamma)$ of the general optical indicatrix of an anisotropic, biaxial mineral. In such cases, we prefer to use the mean, $(\varepsilon_{intX} + \varepsilon_{intY} + \varepsilon_{intZ})/3$, and hence the simple $\varepsilon_{int}$ value for the isotropic case. Our use of the mean values is consistent with the use of mean values for other tensorial properties such as, e.g., the refractive index or transport properties in crystal structures.

Table 2 shows that the "water" contents of the 11 garnet samples differ greatly, by factors up to 68, and that the $\alpha_{int}$ values vary concomitantly, but by factors even up to 359. The integral molar absorptivities, $\varepsilon_{int}$, given in the last column of Table 2 are not constant within the limits of error but differ by factors up to about 7 among the various types of garnets, being lowest in the pyrope–almandine garnet PYRALTAN and highest in the grossular–andradite and–goldmanite garnets HESS1 and TSAV, respectively. In an attempt to comment the results on the molar absorptivities in the various types of garnets studied here, we may state:

1. The wide variation of the molar absorptivities in these different types of garnets is consistent with previous studies (Aines and Rossman 1984a; Rossman et al. 1988; Rossman and Aines 1991).
2. The four grossular-rich garnets HESS1, TSAV, MALI and GRMALI exhibit strongly differring $\varepsilon_{int}$ values, the two first larger by factors of 3 to 6 than those of the two latter ones, which are in the range of the molar absorptivities of the garnets close to the

(PyrAlm) solid solutions. It might be recalled that the $Goss_{ss}$ MALI and GRMALI contain relatively high amounts of the Andr component.

3. The Spess-containing garnets GTLAX and SPESSOR, the latter with a composition close to the end member, do not greatly differ in $\varepsilon_{int}$ from (PyrAlm) solid solutions.
4. The NRA-analyzed "water" contents, as well as the shapes of the spectra of the (PyrAlm) garnets RHOTAN2, PYRALTAN and RHOTAN1, are very similar; nevertheless, integral intensities differ (Table 2; Fig. 3). Also, the $\varepsilon_{int}$ values do not increase in the sequence of Pyr contents. As the three garnets hold nearly the same very low amounts of the Gross and Spess components, the related substitutions cannot explain such a behaviour.

The last three observations are not all in accordance with the earlier studies referred to above. We can think of three contributions of different nature to the wide variability in the $\varepsilon_{int}$ values:

1. The hydroxyl groups might be inhomogeneously distributed in the crystal volume. Then, because of the limited depth range covered by the NRA experiments, the values of the "water" concentration obtained and the ensuring $\varepsilon_{int}$ will not be representative for the entire sample, thus leading to apparent variabilities. A number of arguments show that such effects can be ruled out at least for most of the samples studied here: lateral scans with the IR beam over the samples did not reveal inhomogeneities. In addition, "water" values from NRA on different spots of large garnet plates as well as on the two different sides of the plates agreed within the limits of the error, as stated above. The only example of inhomogeneity of OH distribution as a cause of different $\varepsilon_{int}$ values might be HESS1, where the thick plate yields a lower $\varepsilon_{int}$ value than the thinned one (Table 2). However, here the large difference of $\varepsilon_{int}$ between the two plates is mostly due to a great difference in the $\alpha_{int}$ values (Table 2) so that effect (2) cannot be excluded.

2. Thick plates might produce spectra deformed by truncation of the top of the strongest bands. However, in the spectrum of the thick plate of HESS1, the transmission minimum in the top of the strongest band near 3650 $cm^{-1}$ is situated at 1.8%, a value in excess of the T range where truncation of band tops is normally observed. If truncation of band tops would explain the effect observed in HESS1, then the ratios of band maxima of weak to strong bands will be lower in thick than in the thin plates, which is hardly observed in the HESS1 spectra of Fig. 4, lower part. The intensity ratios of the bands at about 3660 and 3640 $cm^{-1}$ in the spectra, $\alpha_{3660}/\alpha_{3640}$, are 0.63 for the thick and 0.51 for the thin plate. Thus, the top of the strong band at 3640 $cm^{-1}$ may indeed be slightly truncated. However, slight truncation will not significantly alter the total area of $\nu_{OH}$ absorptions, i.e., the total integral absorptivity, $\Sigma\alpha_{int}$. In any case, the $\varepsilon_{int}$ value of the thick plate of HESS1 will not be included in the further discussion.

3. The third contribution might result from the fact that the molar absorptivities of $\nu_{OH}$ bands generally increase with decreasing energy position of the bands or centres of band systems (Paterson 1982; Libowitzky and Rossman 1997). Figure 5 displays a plot of our $\varepsilon_{int}$ values as a function of the centre of gravity of the $\nu_{OH}$ band systems.

Corresponding functions of Paterson (1982) and Libowitzky and Rossman (1997) are also shown, using 1/3 of the $\varepsilon_{int}$ values of the papers referred to in order to be consistent with our above definition. As can be seen from Fig. 5, a potential contribution (3) cannot explain the variability of the $\varepsilon_{int}$ values.

In summary, the variations in the molar absorptivities observed here might be related – at least in part – to still unrevealed relations between the complex garnet compositions and their $\nu_{OH}$ positions and specific intensities.

Regarding absolute values, Fig. 5 shows that the $\varepsilon_{int}$ values of the thin HESS1 sample and of the TSAV garnet are consistent with the values predicted by the function of Paterson (1982), whereas all other garnets exhibit $\varepsilon_{int}$ values appreciably lower than those expected from both functions. This supports previous observations that the molar absorptivity of "water" traces bound in defects in structures of nominally anhydrous minerals – in our case garnets – can be strongly reduced compared to the molar absorptivities of minerals with constitutional "water" (Bell et al. 1995,2003; Maldener et al. 2001) on which the functions referred to were determined. In fact, our data displayed in Fig. 5 might suggest rather a decrease than an increase of $\varepsilon_{int}$ with decreasing $\nu_{OH}$ for the case of non-constitutional "water", as proven by the two functions referred to.

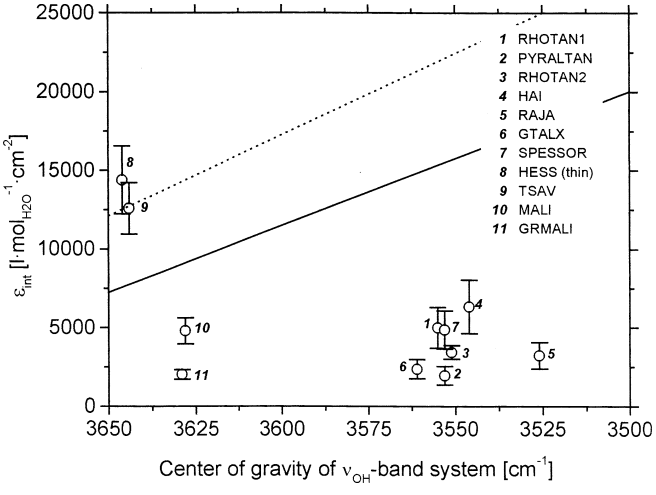


**Fig. 5** Integral molar absorptivities of "water" in garnets of the present study, $\varepsilon_{int}$, in dependence on the energy position of the centre of gravity of the $\nu_{OH}$ band systems in the respective garnet spectra. The dependencies $\varepsilon = f[\nu(cm^{-1})]$ established by Paterson (1982), *dotted line*, and by Libowitzky and Rossman (1997), *solid line*, are shown for comparison. The $\varepsilon_{int}$ values of these functions are multiplied here by 1/3 to have them consistent with our choice of mean integral absorbancies instead of sums (cf. text)

This might be the consequence of the different incorporation mechanisms.

Concerning the practical task of the calibration of the "water" determination in garnets from their single-crystal infrared $\nu_{OH}$ spectra, we suggest here using the average, $\varepsilon_{int} = 3630 \pm 1580 (1 mol^{-1}_{H_2O} cm^{-2})$, which we calculate from our data on nine different garnets (Fig. 5), omitting the close-to-end-member grossular HESS1 and TSAV. This value is lower than the value of 6700 ± 670 ($1\ mol^{-1}_{H_2O} cm^{-2}$) obtained by Bell et al. (1995) on the garnet megacryst MON-9 from the Monastery kimberlite, South Africa. This value is probably the single most accurate one that exists in the literature for a specific garnet, but it should also be kept in mind that this pyropic garnet is chemically somewhat peculiar in that it holds about 20% of its total iron as Fe(III) and has also relatively high titanium contents of 0.06 atpfu, as calculated from its analytical data (Bell et al. 1995; Table 1).

In any case, in the application of the IR method of "water" determination on garnets, one should be aware that the true value can differ by about 50% from that obtained using the proposed value of $\varepsilon_{int}$. On the other hand, the IR method, using molar absorptivities obtained on a broad variety of calibrational samples, has three great advantages: it is relatively simple, provides a very low detection limit at about 2 wt.ppm $H_2O$ and can be performed at high areal resolution with measuring areas down to about 30 × 30 μm.

**Acknowledgements** The authors thank H. Reuff, TU, Berlin, for careful preparation of the crystal plates, S. Herting-Agthe and Ch. Agthe, both TU, Berlin, and S. Greiff, RGZM, Mainz, for providing garnet samples, as well as M. Michaelis and B. Büchtemann, BAM, Berlin, for the RFA analyses. Helpful discussions with E. Libowitzky and M. Andrut, both Univ. Wien, as well as helpful comments and criticism by A. Beran, Wien, and G.R. Rossman, Pasadena, who reviewed the first version of the manuscript, are also gratefully acknowledged. Our thanks are due to the Deutsche Forschungsgemeinschaft, who generously supported the study under grants no. La 324/32 and no. Ra 303/14.

## References

Ackermann L, Cemic L, Langer K(1983) Hydrogarnet substitution in pyrope. a possible location for "water" in the mantle. Earth Planet Sci Lett 62:208–214

Aines RD, Rossman GR (1984a) The hydrous component in garnets: pyralspites. Am Mineral 69:1116–1126

Aines RD, Rossman GR (1984b) Water content of mantle garnets. Geology 12:720–723

Beilby G (1921) Aggregation and flow of solids. McMillan, London

Bell DR, Rossman GR (1992a) The distribution of hydroxyl in garnets from the subcontinental mantle of Southern Africa. Contrib Mineral Petrol 111:161–178

Bell DR, Rossman GR (1992b) Water in Earth's mantle: the role of nominally anhydrous minerals. Science 255:1391–1397

Bell DR, Ihringer PD, Rossman GR (1995) Quantitative analysis of trace OH in garnet and pyroxene. Am Mineral 80:465–474

Bell DR, Rossman GR, Maldener J, Endisch D, Rauch F (2002) Hydroxide in olivine: quantitative determination of the absolute amount and calibration of the IR spectrum. J Geophys Res, *108* (B2), 2105, doi:10.1029/2001JB000679, 2003

Beran A, Libowitzky E (1999) IR spectroscopy and hydrogen bonding in minerals. In: Wright K, Catlow, R(eds). NATO Science Series Kluwer, Dordrecht, 493–508

Beran A, Langer K, Andrut M (1993) Single crystal infrared spectra in the range of OH-fundamentals of paragenetic garnet, omphacite and kyanite in an eclogitic mantle xenolith. Mineral Petrol 48:257–268

Bowden F, Hughes TP (1937a) Surface temperature of rubbing solids and the formation of the Beilby layer. Nature 139:152

Bowden F, Hughes TP (1937b) Physical properties of surfaces. IV. Polishing, surface flow and the formation of the Beilby layer. Proc Roy Soc London (A) 160:575–587

Endisch D, Sturm H, Rauch F (1993) Development of a measuring set-up for high-sensitivity analysis of hydrogen by the 15N nuclear reaction technique. Fresenius Z Anal Chem 337:12–24

Endisch D, Sturm H, Rauch F (1994) Nuclear reaction analysis of hydrogen at levels below 10 at.ppm. Nuclear Instr Meth Phys Res (B) 84:380–392

Geiger CA, Langer K, Bell DR, Rossman GR, Winkler B (1991) The hydroxide component in synthetic pyrope. Am Mineral 76:49–59

Geiger CA, Stahl A, Rossman GR (2000) Single-crystal IR- and UV/VIS-spectroscopic measurements on transition-metal-bearing pyrope: the incorporation of hydroxide in garnet. Eur J Mineral 12:259–271

Langer K, Robarick E, Sobolev NV, Shatsky VS, Wang W (1993) Single-crystal spectra of garnets from diamondiferous high-pressure metamorphic rocks from Kazakhstan indication for OH-, H2O and FeTi charge transfer. Eur J Mineral 5:109–1100

Libowitzky E, Rossman GR (1997) An IR absorption calibration for water in minerals Am Mineral 82:1111–1115

Lu R, Keppler H (1997) Water solubility in pyrope. Contrib Mineral Petrol 129:35–42

Maldener J, Rauch F, Gavranic M, Beran A (2001) OH absorption coefficients of rutile and cassiterite deduced from nuclear reaction analysis and FTIR spectroscopy Mineral Petrol 71:21–29

Matsyuk SS, Langer K (1998) Hydroxyl defects in garnets from mantle xenoliths in Kimberlites of the Siberian platform. Contrib Mineral Petrol 132:163–179

Paterson MS (1982) The determination of hydroxyl by infrared absorption in quartz, silicate glasses and similar materials. Bull Min 105:20–29

Ramsay DA (1952) Intensities and shapes of infrared absorption bands of substances in the liquid phase. J Am Chem Soc 74:22–80

Rossman GR (1996) Studies of OH in nominally anhydrous minerals. Phys Chem Miner 23:299–304

Rossman GR, Aines RD (1991) The hydrous component in garnets: grossular–hydrogrossular. Am Mineral 76:1153–1164

Rossman GR, Rauch F, Livi R, Tombrello TA, Shi CR, Zhou ZY (1988) Nuclear reaction analysis of hydrogen in almandine, pyrope and spessartine garnets. N Jb Miner Mh: 172–178

Rossman GR, Beran A, Langer K (1989) The hydrous component of pyrope from the Dora Maira Massif, Western Alps. Eur J Mineral 1:151–154

Wagner W, Rauch F, Bange K (1989) Concentration profiles of hydrogen in technical oxidic thin films. Fresenius Z Anal Chem 333:478–480